Wood Science & Technology manuscript No.
(will be inserted by the editor)

Numerical Simulation of Pressure-Driven Adhesive Penetration into Realistic Wood Structures

Chad C. Hammerquist and John A. Nairn

Received: July 11, 2018

Abstract The Material Point Method (MPM) was used to numerically model pressure-driven flow of adhesive into hybrid poplar wood. The cellular structure of the hybrid poplar was discretized in an MPM model by converting X-ray computed tomography (XCT) voxels from 3D scans of actual wood-adhesive bond lines into material points in the model. In the MPM model, a slab of adhesive between two wood adherends was forced into the modeled wood structure. The wood material was modeled as a rigid material and the adhesive as a compressible, non-Newtonian fluid. MPM is well suited for these simulations because it can handle the large deformation of the adhesive fluid as well as adhesive-wood contact. The MPM fluid model with contact was verified by 2D simulations of a geometry with a known analytical solution using the same parameters and resolution as the full 3D simulations. Multiple 3D simulations were run and the modeled adhesive penetration at the end of the simulations was compared to experimental penetration observations in the source XCT data. The simulation results correlated well with experimental results.

1 Introduction

Wood is experiencing increased interest among green-minded architects and builders for use as a structural material. If managed properly, wood has the potential to be an eco-friendly and sustainable resource (Upton et al, 2008). Increasing the amount of wood used in construction could play a role in mitigation of the current CO_2 and climate change crisis. Many structural wood products are in the form of engineered wood composites – a class of materials that are manufactured by cutting wood into smaller pieces (*e.g*, veneers, flakes strands, particles) and joining them together with adhesives. Some common examples of wood composites are plywood, oriented strand board (OSB), laminated veneer lumber (LVL), glulam, and cross laminated timber (CLT). A key component in such composites is an adhesive that bonds the wood together and transfers stress throughout the material. In most manufacturing methods, liquid adhesive is applied to wood surfaces and then compressed to form the bond. The compression brings wood surfaces together and forces some amount of adhesive penetration into the porous wood structures.

One view of adhesive penetration is that it provides a mechanism to increase surface contact between adhesive and the wood. This contact may promote a strong bond due to intermolecular and chemical forces as well as mechanical interlocking (Paris et al, 2014). On the other hand, if the adhesive penetrates too far into wood, bond lines may become starved of adhesive resulting in weaker bonds. Excessive penetration also wastes expensive glue by filling regions that provide limited benefit to bond line performance (Paris and Kamke, 2015). Clearly, a detailed understanding of the process of adhesive penetration into wood and the resulting performance of the wood/adhesive bond line is of interest to manufacturers of wood

John A. Nairn
Oregon State University, Wood Science & Engineering
112 Richardson Hall, Corvallis, OR 97330, USA
Tel.: +1-541-737-4265, Fax: +1-541-737-3385, E-mail: John.Nairn@oregonstate.edu

composites. Such understanding would help them develop adhesives that can provide an optimal amount of penetration into a variety of wood species.

This paper describes 3D numerical simulation of adhesive penetration into realistic wood structures. Some researchers have attempted to model average penetration into wood (Mendoza et al, 2012). The analogous problem of resin penetration into fiber mats during resin transfer modeling has been limited to average resin flow using Darcy's law for flow into porous media (Isoldi et al, 2012; Gascón et al, 2016). To our knowledge, this work is the first to undertake simulations of adhesive flow into explicit, 3D wood structures. One similar project used SPH (smooth particle hydrodynamics) methods to model injection of bone cement into porous bone (Basafa et al, 2013).

A detailed 3D model for adhesive penetration into wood (or for flow into any porous media) faces two grand challenges. First, the numerical model must accurately represent the structure of the wood. Attempts to use idealized or simplified models for wood's cellular structure (*e.g.*, an array of hexagonal cells) would give limited insights into adhesive penetration. Any model that hopes to explain penetration differences that depend on wood species or details of wood anatomy (*e.g.*, early wood *vs.* late wood, presence of vessel elements, cell-wall pits, *etc.*) must always use realistic wood structures that contain those features. Second, any proposed simulation method should be validated by comparison to experiments. RTM simulations of average flow have been validated by comparison to 2D experiments on model fiber mats (Oliveira et al, 2016). The comparable experiments for penetration of adhesive into wood are not available (and maybe not possible). Instead, new simulations need to be compared to 3D experiments for adhesive penetration.

Both challenges can be resolved by making use of recent experimental data on 3D adhesive penetration into wood (Paris et al, 2015; Paris and Kamke, 2015; Paris et al, 2013). These experiments used high-resolution X-ray computed tomography (XCT) to observe wood adhesive bonds for several resins and several species. By sufficiently tagging the adhesive for X-ray contrast, the experiments could segment adhesive and wood structure and both visualize and quantify 3D adhesive penetration. These experimental data provided our simulations with both input structures, allowing us to model realistic wood structures, and experimental observations of adhesive penetration, allowing us to validate simulations by direct comparison to experiments.

Our simulations used the material point method (MPM) (Bardenhagen and Kober, 2004; Sulsky et al, 1994b). This method was chosen because of its ability to easily discretize complex wood structures (Brydon et al, 2005; Nairn, 2006; Aimene and Nairn, 2015) and its potential for handling solid-fluid interaction including adhesive/wood contact mechanics. Figure 1 illustrates the steps in our modeling. Figure 1a shows the initial modeled structure. The explicit 3D wood structure was derived from the wood structure in the XCT data. The adhesive that had penetrated into the wood was moved from its position in the XCT data to a slab of adhesive between the two wood adherends. The simulation then compressed the bond allowing the adhesive to penetrate into the wood. Figure 1b shows the developing adhesive structure part way through a simulation while Fig. 1c shows final prediction of adhesive penetration. Because the initial XCT data had penetrated adhesive, the simulation results could be validated by directly comparing to experiments on the identical wood structure. The comparisons were done both by visualization methods and by quantitative calculation of penetration metrics.

2 Numerical Methods

2.1 MPM Simulations

The material point method (MPM) is a particle-based, computational mechanics tool (Bardenhagen and Kober, 2004; Sulsky et al, 1994b). It was used for this work because of its ability to discretize complex structures (wood structures from XCT data) (Brydon et al, 2005; Nairn, 2006; Aimene and Nairn, 2015), the possibility of using liquid particles to handle fluid-solid interactions (Hu et al, 2010; Hamad et al, 2017; Raymond et al, 2015), and new options for dealing with contact (between liquid adhesive and wood cell walls) (Nairn et al, 2018). These simulations modeled some recent 3D, XCT data for wood adhesive bonds (Paris et al, 2015; Paris and Kamke, 2015; Paris et al, 2013). We considered two of their data sets: hybrid poplar (HP) bonded with phenol formaldehyde (PF) adhesive and HP bonded with a polyvinyl

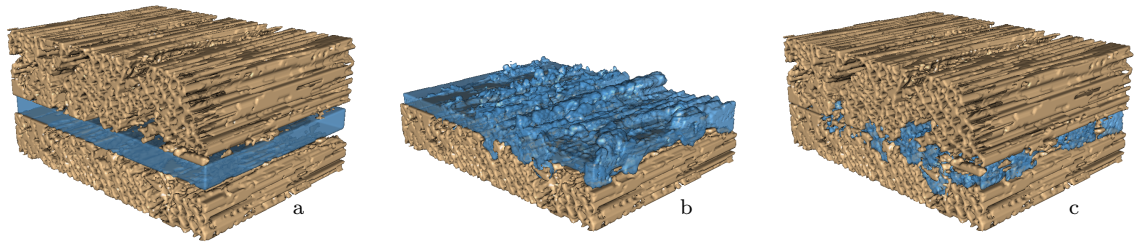

Fig. 1 A rendering of adhesive flow into wood structures predicted by one simulation (this rendering was done using R (R Core Team, 2016) and the `misc3D` package). a. Start of simulation based on actual wood structure with actual amount of adhesive moved to slab between the wood adherends. b. Visualization of adhesive structure part way through the simulations with top wood adherend removed for clarity. c. End of the simulation with 3D predictions for adhesive penetration.

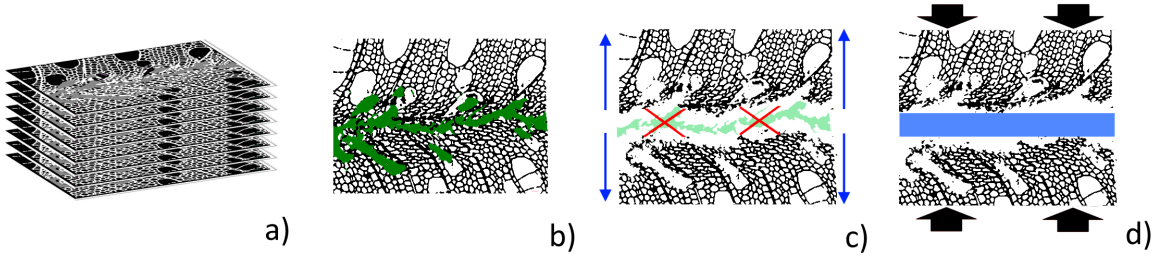

Fig. 2 The simulation framework: a) 2D XCT stack, b) a slice showing the wood structure and experimental results for adhesive penetration, c) region of adhesive is deleted and two sides are separated, d) undeformed glue slab is inserted and the sides are forced together.

acetate/phenol formaldehyde blend (PVA-PF). The XCT data were a stack of 2D images or slices that had been segmented from XCT data into 3 phases: adhesive, wood, and void space. A stack of slices and view of one slice with raw experimental data are in Figs. 2a and b. The resolution of the scans was 1.45 μm^3 per voxel.

The simulations setup is illustrated in Figs. 2c and d. First, the two wood adherends were separated and the adhesive was removed. Second, the adhesive was replaced by a rectangular slab of adhesive between the two adherends; the slab's thickness was chosen such that the total amount of adhesive matched the number of voxels of adhesive in the source XCT data. In real bond formation, the adhesive may shrink after flow and the XCT data would reflect the final volume rather than in the initial volume for the adhesive slab. Because we were not modeling resin shrinkage, however, our only option was to start with final volume of adhesive observed in experiments. Finally, an MPM computer simulation pushed the two adherends together to model clamping and subsequent penetration of glue into the wood structure. Symmetry boundary conditions were applied on the side surfaces to keep adhesive from flowing out the edges. The task of discretizing the complex structures defined by XCT data was solved simply by mapping voxels in the XCT data into material points in the MPM model (Brydon et al, 2005; Nairn, 2006; Aimene and Nairn, 2015).

The cellular structure of HP has long empty channels (*e.g.*, cell lumens and vessel element) that were nearly parallel to the bond line in the studied specimens. For a simulation to capture realistic flow, the model needs enough resolution to allow flow within the lumen space and large enough simulation volume to capture representative features of the wood anatomy (*e.g*, early wood, late wood, vessels, ray cells, *etc.*). Furthermore, wood cells have thin walls, so sufficient resolution is also needed to resolve them as flow barriers. These simulations used a regular MPM grid with cell size of $\Delta x = 2.9$ μm. Each cell had 8 particles resulting in a one to one correspondence between XCT voxels to material points (*i.e.*, each material point's initial volume was 1.45 μm^3) and providing the maximum resolution available from source XCT data. Figure 3 illustrates this resolution by showing typical number of grid cells across

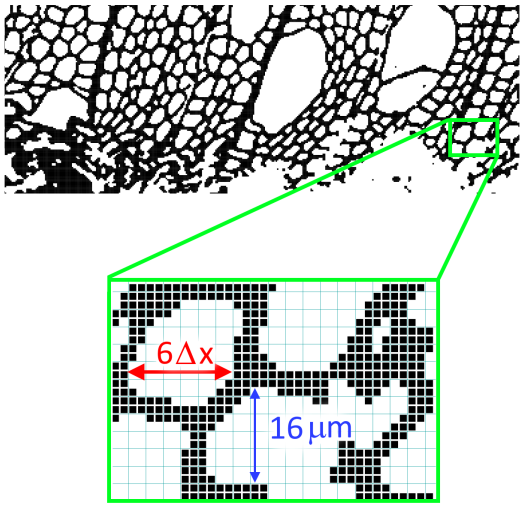

Fig. 3 A zoomed view of a portion of a 2D cross-section of the wood structure made up wood cell wall material points (rigid material points as black squares showing cross section of particle with volume 1.45 μm^3). The background lines show MPM grid cell lines that are cross sections of cubical cells having volume of 2.9 μm^3.

small lumens and number of particles across cell walls. The cross section of each slice was 0.57 mm × 0.57 mm and about 400 slices were used to simulate a total length along the bond line of 0.58 mm. The resulting simulations contained approximately 17 million particles. Visual inspection showed this volume element reflects many features of HP anatomy, including wood cells, ray cells, and vessel elements. We used the MPM code OSParticulas (which is development version of the public domain NairnMPM code (Nairn, 2016)). The simulations took between 10 and 30 days depending on adhesive, wood structure, and resulting clamping speed. OSParticulas is parallel code and was run on single server nodes with 24 to 32 cores.

2.2 Modeling Wood, Adhesive, and Wood-Adhesive Contact

The wood cell walls were modeled as a rigid material, with the assumption being that the wood is much more rigid than a liquid and most of the interesting physics is happening in the liquid region. The use of rigid materials allowed for faster simulations. Modeling the wood structure as an elastic material would require smaller time steps, because the stiffness of wood is higher than the fluid. Also, rigid materials need far fewer calculations during the simulations — the only calculations were to move them at a prescribed velocity and to extrapolate them to the grid to model contact with the fluid (see below).

The use of rigid wood properties, however, imposes some limitations. The XCT data provides evidence of localized crushing of the wood cell walls near the bond line. In other words, real clamping methods can deform cell walls, but no such deformation occurs when using rigid materials. Because our MPM model was based on XCT data, these simulations modeled penetration into a wood surface that may have initial damage. It would be preferable to simulate penetration into undamaged wood (or just damage caused by surface preparation methods), but we did not have XCT data for specimens prior to bonding. The main goal of this work was to validate penetration simulations by comparing computer predictions to XCT experiments on penetration; the only available XCT data for such validation required use of post-bonded wood, which may include some damage caused during bonding. Future work should start with undamaged wood and include wood deformation during the clamping process.

When using rigid materials, a simulation prescribes their velocity and updates their positions in each time step. We chose a closing speed of 1 m/s, which was a rough estimate of closing speed for a high-speed laminated veneer lumber (LVL) processing line where veneer layers are compressed from an initial stack to final thickness by passing through rollers. Other wood processing methods likely have slower clamping speeds. When this clamping speed was kept constant, the net clamping pressure (measured by contact

Table 1 Experimental results for viscosity of the PVA-PF blend adhesive as a function of shear rate.

$\log_{10}(\dot{\gamma}(s^{-1}))$	η (cP)
0	210,000
0.8	87,000
1.6	1700
2.7	1000
∞	1000

forces as described below) increased beyond physical limits for wood. To avoid such unrealistic forces, a load controlling PID (Proportional, Integral, Derivative, controller, see Graf (2016)) feedback loop was used to dynamically adjust the velocity of the rigid particles to keep pressures at or below the compression strength of HP (2.5 MPa (Robert J. Ross; USDA Forest Service., 2010)). This compression strength also corresponds to formation of cell wall buckling during deformation (Gibson and Ashby, 1982), but far below pressures required to start densifying the pore space (Nairn, 2006).

The adhesive in these simulations was modeled as a non-Newtonian, compressible fluid. The pressure was modeled as a Tait fluid (Li, 1967) where pressure is given by:

$$p = CK\left[\exp\left(\frac{1}{C}\left(1-J\right)\right)-1\right] \tag{1}$$

where $C = 0.0894$ is a universal Tait constant, K is bulk modulus, and J is the determinant of the deformation gradient, or relative volume V/V_0. The shear (or deviatoric) stress as a function of the deviatoric, symmetrized velocity gradient of the fluid was modeled using:

$$\tau = \eta(\dot{\gamma})\left(\nabla\mathbf{v}+\nabla\mathbf{v}^T-\frac{2}{3}\mathrm{Tr}(\nabla\mathbf{v})\mathsf{I}\right) = 2\eta(\dot{\gamma})\mathrm{dev}(\nabla\mathbf{v}) \tag{2}$$

where $\nabla\mathbf{v}$ is the velocity gradient and $\eta(\dot{\gamma})$ is the viscosity which can be a function of the shear rate $\dot{\gamma} = 2|\mathrm{dev}(\nabla\mathbf{v})|$. The full stress tensor combines these constitutive laws for Cauchy stress of $\sigma = -p\mathsf{I}+\tau$.

The modeled PF adhesive had a measured density of $\rho = 1.2$ g/cm^3 and a measured viscosity of $\eta = 1300$ cP. The viscosity was measured at multiple shear rates and found to be constant (Paris and Kamke, 2015); thus PF was modeled as a Newtonian, compressible fluid. The bulk modulus K was not measured, but was set to 1 GPa for the simulations. This bulk modulus might be lower than most fluids, but it is on the same order of magnitude. Furthermore, the use of a lower bulk modulus allows larger time steps and faster simulations. The modeled PVA-PF adhesive blend had a measured density of $\rho = 1.2$ g/cm^3 and measured viscosity that depended on shear rate (Paris and Kamke, 2015). The experimental results for viscosity were fit to a piecewise log model. The properties used are shown in Table 1. Simulated shear rates between two table values were found by linear extrapolation in $\log_{10}(\dot{\gamma})$. The bulk modulus K for PVA-PF was also set to 1 GPa.

Contact between adhesive and wood (or between liquid and solid) was modeled using multi-material mode MPM with contact algorithms (Bardenhagen et al, 2001; Nairn, 2013; Nairn et al, 2018). In multi-material mode MPM, each material has its own velocity field on the grid and contact laws are implemented on nodes that share more than one material type. Most prior MPM contact has been limited to frictional or stick contact (Bardenhagen et al, 2001; Nairn, 2013). We used a recent generalization of MPM contact laws (Nairn et al, 2018) to implement a partial slip model where the shear stress at a contacting surface is given by:

$$\tau_w = \eta(\dot{\gamma}_w)\dot{\gamma}_w = k\eta(k\Delta v_t)\Delta v_t \tag{3}$$

where $\dot{\gamma}_w$ is the shear rate at the contacting surface. This shear rate is found from $\dot{\gamma}_w = k\Delta v_t$ where k is a constant with units 1/length and Δv_t is the sliding (or tangential) velocity difference between the two materials. The parameter k has physical interpretation as a "influence" zone near the surface. This contact law can model slip conditions ($k = 0$, $\tau_w = 0$, or frictionless), stick conditions ($k \to \infty$ or $\Delta v_t \to 0$), or anything in between ($0 < k < \infty$) as partial slip. Simulations were run with $k = 0$ (frictionless) and $k = (0.01\Delta x)^{-1}$ where $\Delta x = 2.9$ μm was the grid resolution (partial slip).

Adhesive-wood contact may also result in capillary forces that could suck resin into lumens or resist penetration of resin depending on contact angle θ between cell wall and resin. Energy balance methods estimate the capillary pressure drop as (Mortensen and Cornie, 1987; Michaud, 2016):

$$\Delta P = -S_f \gamma \cos\theta \tag{4}$$

where S_f is wood-resin contact area per unit volume and γ is surface tension of the resin. Estimating $S_f = 2/r$, where r is lumen radius, and $\gamma = 0.03$ N/m for typical adhesives, $\Delta P = -2.4\cos\theta$ kPa. This estimated capillary force is $1000\times$ lower than clamping pressure and can be neglected. Future simulations at lower pressures (*e.g.*, modeling capillary flow only) or maybe with lower viscosity resins might need to add surface tension effects. The feature is currently not available in our liquid-solid, MPM modeling.

MPM contact is implemented by calculating the change in momentum for each material velocity field on a contact node to satisfy the chosen contact mechanics with other materials(Bardenhagen et al, 2001; Nairn, 2013; Nairn et al, 2018). A change in momentum per unit time corresponds to a contact force (Nairn et al, 2018). We summed contact forces for all rigid materials on one side of the bond to monitor the net clamping pressure. This contact pressure was used in the PID feedback loop to control velocity such that total clamping pressure did not exceed the transverse compression strength of wood.

2.3 Verification of Adhesive Modeling

To verify our MPM fluid modeling at a resolution corresponding to modeled lumen space, we ran 2D, plane strain simulations using PF fluid properties. A block of fluid was allowed to flow under gravity down a 50° inclined plane (see top-left of Fig. 4). The rigid surface was horizontal, but body forces were applied at 40° to model the incline. The fluid boundary conditions were stick conditions with the rigid material on the bottom and stress-free on the top. To compare to lumen space resolution, a 17.4 μm thick layer was modeled with 6 grid cells (see Fig. 3). This inclined-flow problem was chosen because an analytical solution is easily obtained by solving the Navier-Stokes equation for a Newtonian fluid with the prescribed boundary conditions:

$$v(y) = -\left(\frac{\sin(\theta)\rho g}{\eta}\right) y \left(\delta - \frac{y}{2}\right) \tag{5}$$

where y is normal distance from the surface, g is applied body force, ρ and η are the fluid's density and viscosity, and δ is fluid layer thickness Wilkes (2006). We used g higher than gravity to help induce the high-viscosity fluid to flow in a reasonable time.

Our first verification simulation used standard MPM methods (denoted here as FLIP standing for Fluid Lagrangian Implicit Particle (Brackbill and Ruppel, 1986; Sulsky et al, 1994a; Hammerquist and Nairn, 2017)). The velocity profile of the flow at 0.5 ms measured on the grid in the middle of the fluid (to avoid boundary effects) is compared to the analytical solution in Fig. 4. The FLIP velocities smoothed to the grid exactly reproduce the analytical solution, but FLIP simulations of fluids develop considerable noise in the distribution of particle velocities (see 4). Such noise may limit the reliability and stability of complex, 3D, glue penetration simulations.

MPM codes have a reputation of being noisy in fluid simulations (Hammerquist and Nairn, 2017). This noise is a consequence of a mismatch in degrees of freedom between the background grid and the particles. The noise can build up and limit simulation accuracy. A new MPM technique named XPIC(m) (of order m) was recently developed to address this problem (Hammerquist and Nairn, 2017). In brief, XPIC(m) provides an alternative method for updating particle velocities. All orders of XPIC(m) force the grid and particles to have the same effective degrees of freedom. Low orders of XPIC(m) reduce noise, but may add unwanted damping. XPIC(1) is equivalent to PIC (or Particle in Cell method), which is known to cause over damping of fluids (Brackbill et al, 1988; Hammerquist and Nairn, 2017; Jiang et al, 2017). Higher orders of XPIC(m) approach the limit of damping only frequencies not seen by the grid (*i.e.* removal of only null space noise), with the trade off being computational cost.

We found XPIC(5) to be a good compromise between limiting unwanted damping and minimizing computational cost. Figure 4 shows velocity profile and distributions of particle velocities for XPIC(5)

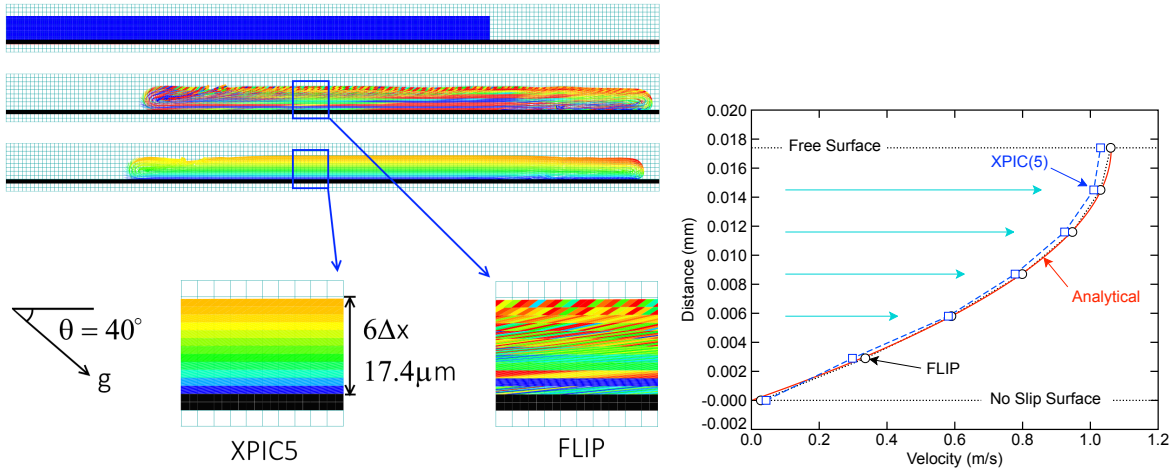

Fig. 4 Left) The 2D fluid simulations. Black particles are rigid material that interact by contact. The blue rectangle is the initial fluid region, then XPIC and FLIP solutions are shown after 0.5 ms. Fluid particles are colored with relative velocity (blue for zero to red for maximum velocity). Right) Velocity of profile of simulations compared to analytical solution.

simulations of fluid on an inclined surface. The velocity profile is nearly exact, although shows a slight amount of damping near the maximum velocity. Compared to FLIP, the spatial variations in XPIC(5) velocities are excellent and virtually free of noise. All simulations in this work were run by both FLIP and XPIC(5). The FLIP results were used to confirm that XPIC(5) does not over damp. The XPIC(5) simulations had less noise and more stable simulations that were preferred for post-analysis of results.

3 Results and Discussion

This study consisted of three PF and three PVA-PF full-scale, 3D simulations. Two PF simulations used partial slip contact between liquid and wood with either FLIP velocity or XPIC(5) velocity update; a third PF simulation used frictionless contact with FLIP velocity update. The same set of three simulations were run for the PVA-PF adhesive.

Clamping pressures *vs.* time for all simulations are shown in Figs. 5 and 6. The PF simulations started with the two wood sections separated by 55.1 μm and moving together at 1 m/s. Fig. 5 shows that pressure reached the imposed maximum value of 2.5 MPa early in the simulation causing the velocity to decrease due to feedback control. A consequence of the reduced velocity is that these two PF simulations took the most time. The "Partial Slip" simulations by FLIP and XPIC(5) were nearly identical except the XPIC(5) results had less noise. The "Frictionless" results (done by FLIP) had lower clamping pressure as frictionless sliding reduces the resistance to clamping. In fact, the pressure only barely reached 2.5 MPa. The wood adherends were stopped when the wood sections returned to their original position in the source XCT data. The partial slip simulations never reached the initial position; the frictionless simulations reached initial position at 0.054 ms.

The PVA-PF simulations started with the two wood sections separated by 78.3 μm and moving together at 1 m/s. None of the pressures ever reached 2.5 MPa; thus the clamping speed was held constant at 1 m/s until the adherends returned to their original position in the source XCT data (at 0.078 ms). Like the PF results, the "Partial Slip" results by FLIP and XPIC(5) were similar. The PVA-PF had less noise that could be removed by the XPIC(m) method. Also similar to PF results, the "Frictionless" results (done by FLIP) had lower pressure.

A good way to compare simulation results to experimental results, is to visually compare the final adhesive distribution. The 3D geometry of the adhesive component of the bonds are compared to experimental penetration results in Fig. 7. The geometries from the PVA-PF simulations agreed very well with the experimental geometry. In fact, the simulated and experimental geometries are nearly identical

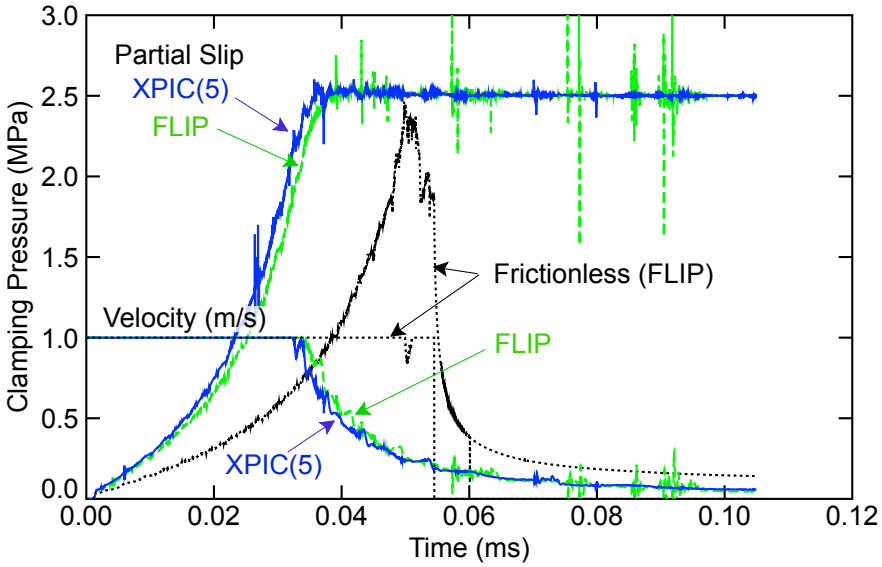

Fig. 5 Plots of the clamping pressure *vs.* time for the three PF simulations — partial slip using XPIC(5) (blue line), partial slip using FLIP (green line), and frictionless using FLIP (black line). The closing velocities (in m/s) for each simulations are plotted with the corresponding line style. Note that velocities automatically decrease to prevent clamping pressure from exceeding 2.5 MPa.

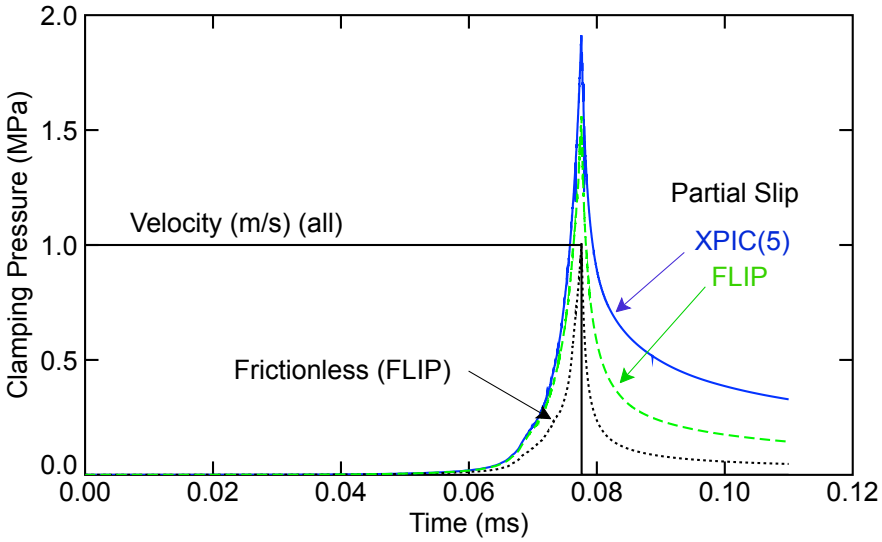

Fig. 6 Plots of the clamping pressure *vs.* time for the three PVA-PF simulations — partial slip using XPIC(5) (blue line), partial slip using FLIP (green line), and frictionless using FLIP (black line). The closing velocities (in m/s) were the same for all simulations (solid black line) and dropped to zero once the gap returned to position in XCT data.

except for a few disconnected points in the experimental geometry that are not seen in the simulations. These points may be regions that were reached from penetration regions beyond the modeled volume element or reached by penetration through openings not resolved in the XCT data.

The PF simulations have regions of good agreement and regions that do not agree as well with experiments (see fig. 7). The disagreement on the bottom-left is due to a large tube of adhesive in the experimental geometry that is not filled in the simulations. It is likely this tube was not well connected to the bond line within the modeled volume element but was instead filled by adhesive that entered the

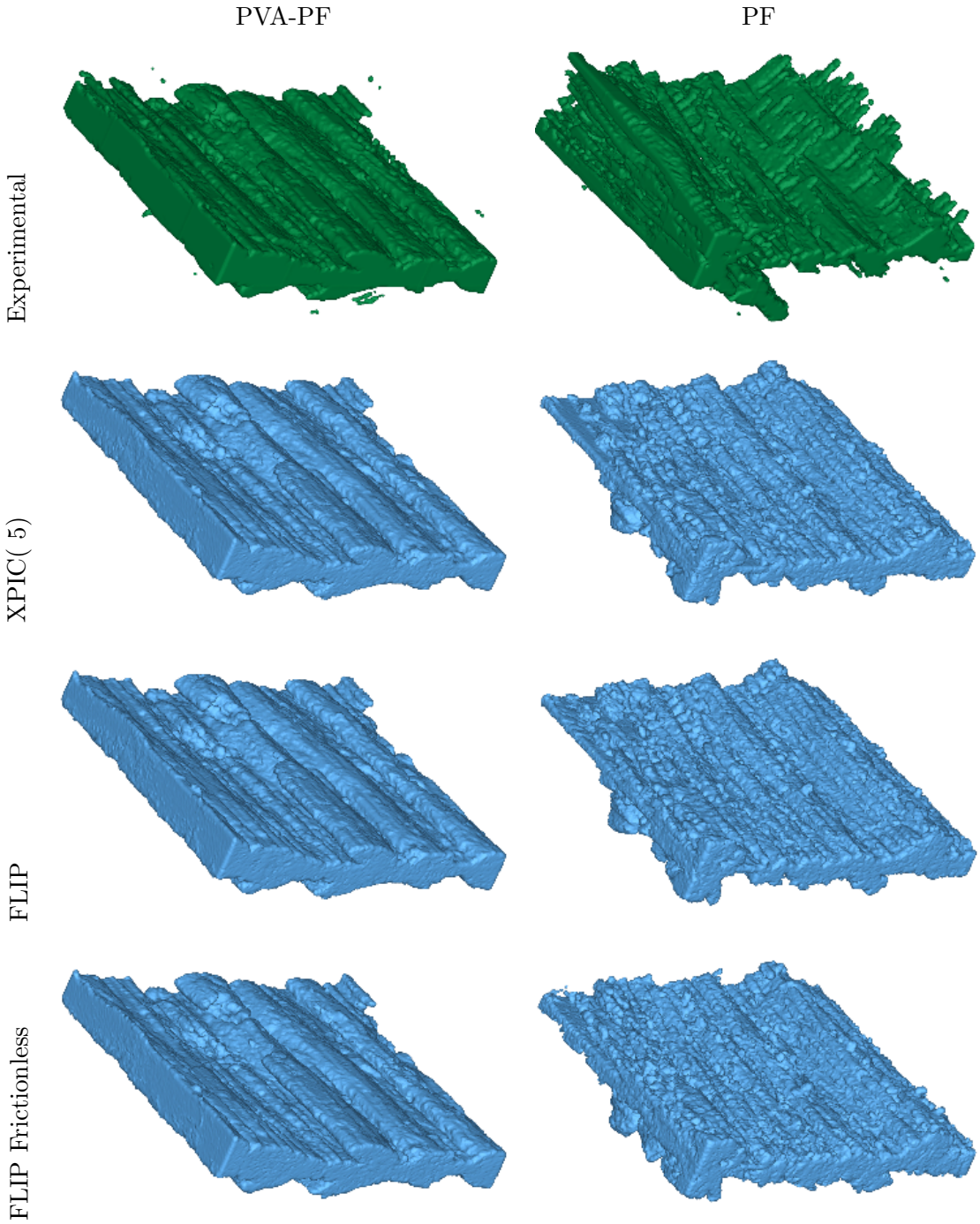

Fig. 7 Visual comparison of experimental results for adhesive penetration (top row) to simulations by partial slip with XPIC (5) (second row), partial slip with FLIP (third row), and frictionless with FLIP (bottom row). The PVA-PF simulations are on the left; the PF simulations are on the right. The plots show only the adhesive component of the 3D experimental and simulations results; the wood component has been removed for clarity.

Table 2 Comparison of bulk weighted penetration (WP) for PVA-PF and PF experiments and simulations. All WP are in μm. XPIC(5) and FLIP were "Partial Slip" results and the "Frictionless" results were done using FLIP.

	PVA-PF			PF		
	Bottom	Top	Total	Bottom	Top	Total
Experimental	24.69	25.96	25.3	68.57	31.62	56.41
XPIC(5)	25.21	23.32	24.35	27.98	27.3	27.7
FLIP	25.18	23.3	24.32	27.97	27.42	27.74
Frictionless	25.24	23.3	24.35	26.57	26.6	26.58

tube outside the simulated region and flowed into the region from the side. Alternatively, the connection may have been closed by damage to the wood cell walls during bonding. Capturing this extra penetration would require modeling a larger section of the bond line or modeling penetration into undamaged wood. Another reason the PF simulations agree less well with the experimental results may be the intricacy of the experimental geometry. Looking at the experimental shape, there are some intricate details on the upper-right side, which are likely ray cells allowing transverse penetration. These cells are either closed off to flow or beyond the resolution of the liquid particles used in the simulations (the liquid particles were 1.45 μm^3). Perhaps using smaller liquid particles along with a finer background mesh, could capture these extra details, but the simulations would be longer.

For numeric comparison between simulations and experiments, we used the weighted penetration metric proposed by Paris and Kamke (Paris and Kamke, 2015). This weighted penetration (WP) is defined as

$$\mathrm{WP} = \sqrt{\frac{\sum_i V_i Y_i^2}{\sum_i V_i}} \tag{6}$$

where Y_i is the perpendicular distance from adhesive voxel i to the bond line and V_i is its volume. In simulations, Y_i and V_i correspond to adhesive materials points. A comparison of this metric for experiments and simulations is in Table 2. The "Top" and "Bottom" metrics considered only adhesive on one side of the bond line while "Total" metric averaged over all locations. These values show that PVA-PF simulations agreed well with experimental geometries while PF simulations had discrepancies. In particular, the tube that is filled with adhesive in experiments caused poor agreement on the "Bottom" surface and in "Total" results. The results for the "Top" surface were better.

Another use of WP is to plot its spatial variation — see Figs. 8 and 9. These plots present WP as a function of position viewed from above or below the bond line surface in a direction normal to that surface. The results for PVA-PF simulations, shows that the simulations agreed in rather fine detail with all experimental results. The plots for PF simulations reveals information on why these simulations did not do as well. In the right part of the domains, the simulations agreed fairly well with the experimental results, but on the left side, there is poor agreement. Comparing this result with the visualization in Fig. 7, the disagreement was caused by the large tube of adhesive, which is likely not connected to the bond line within the modeled volume. Failing to fill this tube is probably why the PF simulations were unable to completely close the gap between the wood structures. The simulations used the same number of voxels of adhesive found in experiments for the slabs of adhesive between the adherends. Because the simulations did not have access to the large tube filled in experiments, the simulation results in more adhesive confined to other regions in the bond line. This extra adhesive resulted in higher clamping forces and prevented full closure (at least without needing excessive pressure).

A benefit of glue-penetration simulations is that one can interrogate the results to gain insights into formation of wood adhesive bonds. For example, we monitored shear rates experienced by the adhesive during the clamping process. Knowing these shear rates could be useful for manufacturers when designing new adhesive blends that have shear-rate dependent rheology. Contour plots of shear rates are plotted as a function time in Figs. 10 and 11. The plots were from partial slip simulations using XPIC(5) because they had reduced noise and better results for distributions of shear rates. The contours represent distributions of shear rates; the thick line is the median shear rate. The lower-viscosity, Newtonian PF resin had consistently high shear rates. The shear rates started to drop around 0.03 ms when the feedback force control led to reduced clamping speed. The non-Newtonian PVA-PF resin started with lower shear rates,

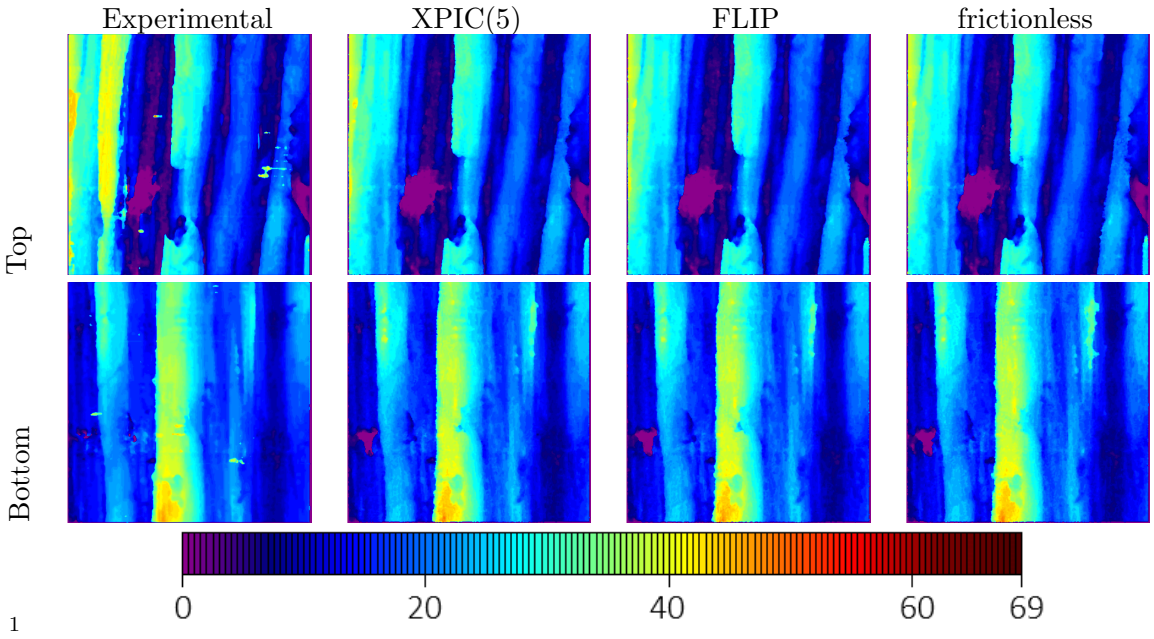

Fig. 8 Comparison of weighted penetration perpendicular to the bond line for the PVA-PF adhesive geometry. Units are in μm.

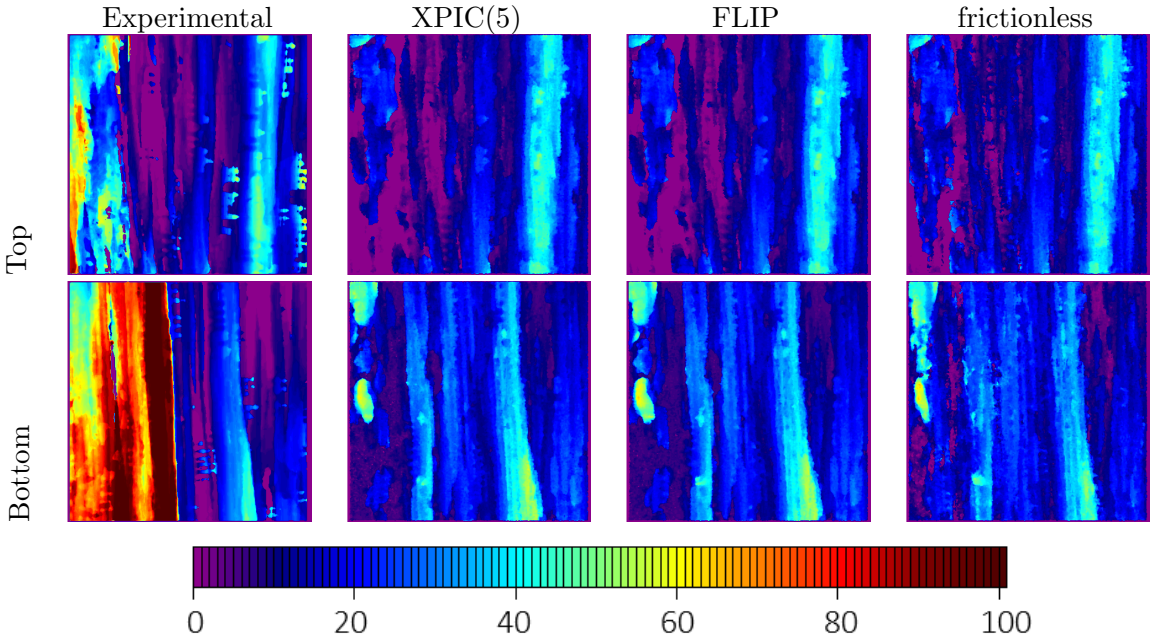

Fig. 9 Comparison of weighted penetration perpendicular to the bond line for the PF adhesive geometry. Units are in μm.

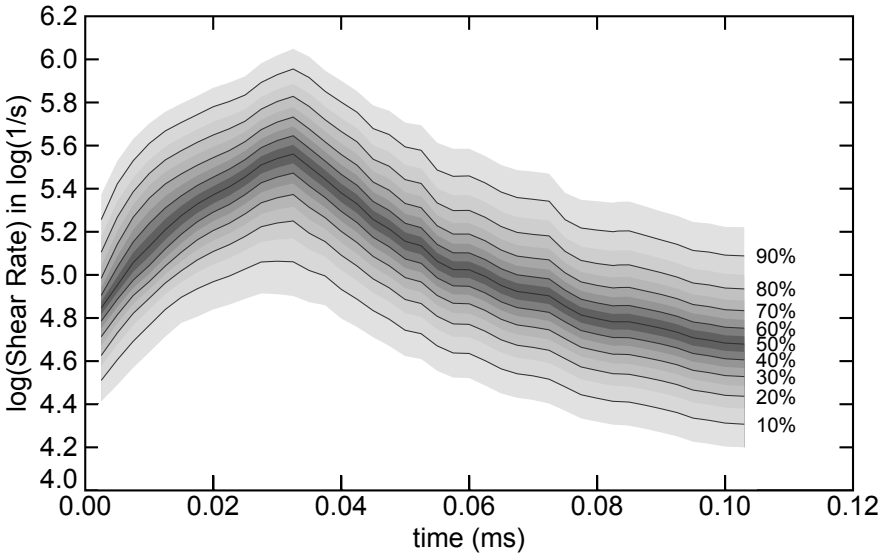

Fig. 10 Quantiles of shear rates vs time during XPIC simulation of the PF geometry.

but approached similar shear rates to PF as the clamping process proceeded. These shear rates decreased when the wood clamping was stopped. Note that at high shear rates, the viscosity of PVA-PF becomes similar to the viscosity of PF. As a result, the peak shear rates were also similar.

The simulation shear rates can be compared to shear rates seen by flow with velocity v through a tube with diameter d (Wilkes, 2006):

$$\dot{\gamma} = \frac{8v}{d} \tag{7}$$

For $v = 1$ m/s through a 50 μm diameter cell lumen, expected shear rates are on the order of 10^5 s^{-1}. This value agrees with median value for PF (Fig. 10) and corresponds to maximum value for PVA-PF (Fig. 11). Slower clamping methods would have correspondingly lower shear rates, but the narrow lumens (d in denominator or Eq. (7)) contribute to high shear rates relative to clamping speeds.

Another option for interrogating the data, would be to input the wood/adhesive structure into a second simulation to study the mechanical properties of the wood adhesive bond. For example, perhaps an MPM damage mechanics (Nairn et al, 2017) model could predict bond failure. The potential simulation options would be to vary wood structure (*e.g.*, different species or different amounts of early wood and late wood), adhesive rheology, clamping conditions, and cure-induced residual stresses and study how such variables affect deformation and fracture of wood adhesive bonds. This current study was limited to XCT of wood adhesive bonds because we required experimental results of adhesive penetration to be able to validate the simulation process. Computer modeling of bond performance, which will be the topic of future publications, would still need detailed XCT data for wood structures of various species, but it would not be limited to XCT data of adhesive bonds. It could use any sufficiently-resolved source of 3D wood structure.

4 Conclusions

By direct comparison of simulated adhesive penetration into wood structures to 3D experimental results on adhesive penetration into the identical structure, we verified that material point method (MPM) simulations are capable of predicting many, but not all, details of glue penetration. For the PVA-PF adhesive, the simulated and experimental results agreed very well by all metrics used to analyze the results. For the PF adhesive, the comparisons were not as good, but the discrepancies can be explained by a few details of the wood structure. The PF simulations failed to predict penetration into regions that were not connected to the bond line within our modeled volume element and missed some fine resolution

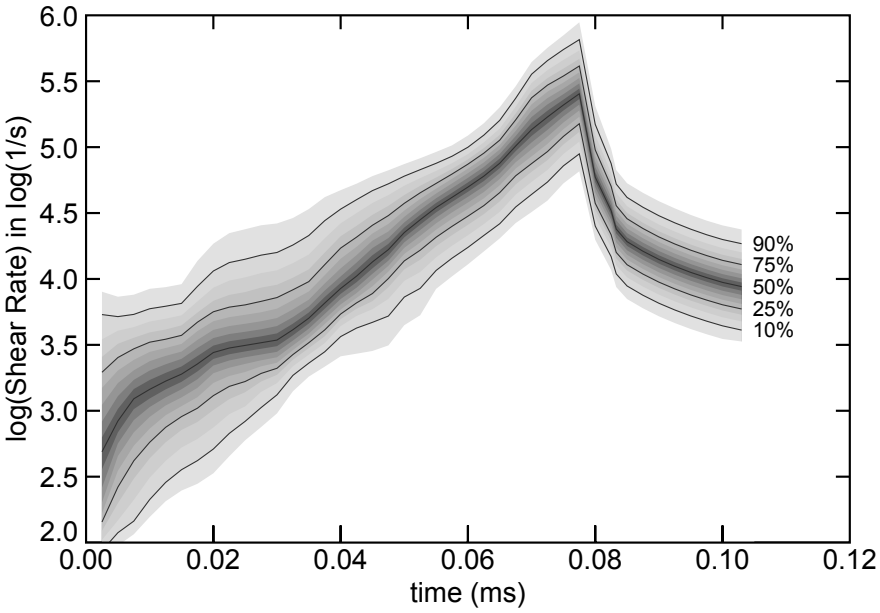

Fig. 11 Quantiles of shear rates vs time during XPIC simulation of the PVA-PF geometry.

features. We expect the discrepancies could be resolved by analyzing a larger volume element, considering undamaged wood, or using higher resolutions. Using a larger volume would not be difficult, but using higher resolution might be beyond current computer capabilities (each doubling of resolution in dynamic 3D simulations increases computational time 16 fold).

These first simulations were interrogated to gain insight in the adhesive conditions during typical clamping conditions. The adhesive experiences a distribution of shear rates reaching maximum values in the range of 10^5 s^{-1}. Future work could investigate topics such as role of wood species, role of wood structure (early wood *vs.* late wood), role of adhesive rheology, and role of clamping rate and pressure. By developing additional simulation methods to predict bond failure, the approach may provide insight into role of all such variables on wood adhesive performance.

Acknowledgements Financial support was provided by the Wood-Based Composites Center, a National Science Foundation Industry/University Cooperative Research Center (Award 1624599-IIP)

References

Aimene YE, Nairn JA (2015) Simulation of transverse wood compression using a large-deformation, hyperelastic-plastic material model. Wood Science and Technology 49:21–39, DOI 10.1007/s00226-014-0676-6

Bardenhagen S, Guilkey JE, Roessig K, Brackbill J, Witzel W, Foster J (2001) An improved contact algorithm for the material point method and application to stress propagation in granular material. CMES: Computer Modeling in Engineering & Sciences 2(4):509–522

Bardenhagen SG, Kober EM (2004) The generalized interpolation material point method. Computer Modeling in Engineering & Sciences 5:477–496

Basafa E, Murphy RJ, Kutzer MD, Otake Y, Armand M (2013) A particle model for prediction of cement infiltration of cancellous bone in osteoporotic bone augmentation. PLOS ONE 8(6):1–10

Brackbill J, Kothe D, Ruppel H (1988) FLIP: A low-dissipation, particle-in-cell method for fluid flow. Computer Physics Communications 48(1):25 – 38

Brackbill JU, Ruppel HM (1986) FLIP: A method for adaptively zoned, particle-in-cell calculations of fluid flows in two dimensions. Journal of Computational Physics 65(2):314 – 343

Brydon AD, Bardenhagen SG, Miller EA, Seidler GT (2005) Simulation of the densification of real open-celled foam microstructures. J Mech Phys of Solids 53(12):2638–2660

Gascón L, García JA, LeBel F, Ruiz E, Trochu F (2016) A two-phase flow model to simulate mold filling and saturation in resin transfer molding. International Journal of Material Forming 9(2):229–239

Gibson LJ, Ashby MF (1982) The mechanics of three-dimensional cellular materials. Proceedings of The Royal Society of London, Series A: Mathematical and Physical Sciences 382(1782):43–59

Graf J (2016) PID Control Fundamentals. Createspace Independent Publishing Platform, URL `https://books.google.com/books?id=kMoEvgAACAAJ`

Hamad F, Wieckowski Z, Moormann C (2017) Interaction of fluid–solid–geomembrane by the material point method. Computers and Geotechnics 81:112 – 124

Hammerquist CC, Nairn JA (2017) A new method for material point method particle updates that reduces noise and enhances stability. Computer Methods in Applied Mechanics and Engineering 318:724 – 738

Hu P, Xue L, Mao S, Kamakoti R, Zhao H, Dittakavi N, Ni K, Wang Z, Li Q (2010) Material point method applied to fluid-structure interaction (FSI)/aeroelasticity problems. In: 48th AIAA Aerospace Sciences Meeting Including the New Horizons Forum and Aerospace Exposition, American Institute of Aeronautics and Astronautics

Isoldi LA, Oliveira CP, Rocha LA, Souza JA, Amico SC (2012) Three-dimensional numerical modeling of RTM and LRTM processes. Journal of the Brazilian Society of Mechanical Sciences and Engineering 34(2):105–111

Jiang C, Schroeder C, Teran J (2017) An angular momentum conserving affine-particle-in-cell method. Journal of Computational Physics 338:137 – 164

Li YH (1967) Equation of state of water and sea water. J geophys Res 72(10):2665–2678

Mendoza M, Hass P, Wittel FK, Niemz P, Herrmann HJ (2012) Adhesive penetration of hardwood: a generic penetration model. Wood Science and Technology 46(1):529–549

Michaud V (2016) A review of non-saturated resin flow in liquid composite moulding processes. Transport in Porous Media 115(3):581–601

Mortensen A, Cornie JA (1987) On the infiltration of metal matrix composites. Metallurgical and Materials Transactions A 18(6):1160–1163

Nairn J (2013) Modeling imperfect interfaces in the material point method using multimaterial methods. Comput Model Eng Sci 1(1):1–15

Nairn JA (2006) Numerical simulations of transverse compression and densification in wood. Wood and Fiber Science 38:576–591

Nairn JA (2016) Material point method (NairnMPM) and finite element analysis (NairnFEA) open-source software. http://osupdocs.forestry.oregonstate.edu/index.php/Main_Page, URL `http://osupdocs.forestry.oregonstate.edu/index.php/Main\_Page`

Nairn JA, Hammerquist CC, Aimene YE (2017) Numerical implementation of anisotropic damage mechanics. International Journal for Numerical Methods in Engineering pp n/a–n/a, DOI 10.1002/nme.5585, URL `http://dx.doi.org/10.1002/nme.5585`, nme.5585

Nairn JA, Bardenhagen SG, Smith GS (2018) Generalized contact and improved frictional heating in the material point method. Computational Particle Mechanics 5(3):285–296

Oliveira I, Amico S, Souza J, Lima A (2016) Resin transfer molding process: a numerical and experimental investigation. The International Journal of Multiphysics 7(2)

Paris JL, Kamke FA (2015) Quantitative wood–adhesive penetration with x-ray computed tomography. International Journal of Adhesion and Adhesives 61:71–80

Paris JL, Kamke FA, Nairn J, Muszyński L, Schwarzkopf M (2013) Wood-adhesive penetration: Non-destructive, 3d visualization and quantification. In: Frihart CR (ed) Proceedings of the international conference on wood adhesives, Toronto, ON, Forest Products Society

Paris JL, Kamke FA, Mbachu R, Gibson SK (2014) Phenol formaldehyde adhesives formulated for advanced x-ray imaging in wood-composite bondlines. Journal of Materials Science 49(2):580–591

Paris JL, Kamke FA, Xiao X (2015) X-ray computed tomography of wood-adhesive bondlines: attenuation and phase-contrast effects. Wood Science and Technology 49(6):1185–1208

R Core Team (2016) R: A language and environment for statistical computing, https://www.R-project.org/. R Foundation for Statistical Computing, Vienna, Austria

Raymond S, Aimene Y, Nairn J, Ouenes A, et al (2015) Coupled fluid-solid geomechanical modeling of multiple hydraulic fractures interacting with natural fractures and the resulting proppant distribution. In: SPE/CSUR Unconventional Resources Conference, Society of Petroleum Engineers

Robert J Ross; USDA Forest Service FPL (2010) Wood handbook : wood as an engineering material. USDA Forest Service, Forest Products Laboratory, General Technical Report FPL- GTR-190, URL https://books.google.com/books?id=v0whAAAAMAAJ

Sulsky D, Chen Z, Schreyer H (1994a) A particle method for history-dependent materials. Computer Methods in Applied Mechanics and Engineering 118(1):179 – 196

Sulsky D, Chen Z, Schreyer HL (1994b) A particle method for history-dependent materials. Comput Methods Appl Mech Engrg 118:179–186

Upton B, Miner R, Spinney M, Heath LS (2008) The greenhouse gas and energy impacts of using wood instead of alternatives in residential construction in the united states. Biomass and Bioenergy 32(1):1 – 10

Wilkes J (2006) Fluid Mechanics for Chemical Engineers with Microfluidics and CFD. Prentice Hall International Se, Prentice Hall Professional Technical Reference